Article

The Structure of the Homogeneous Oxidation Catalyst, Mn(II)(Br), in Supercritical Water: An X-ray Absorption Fine-Structure Study

Yongsheng Chen, John L. Fulton, and Walter Partenheimer

J. Am. Chem. Soc., **2005**, 127 (40), 14085-14093• DOI: 10.1021/ja053421v • Publication Date (Web): 17 September 2005

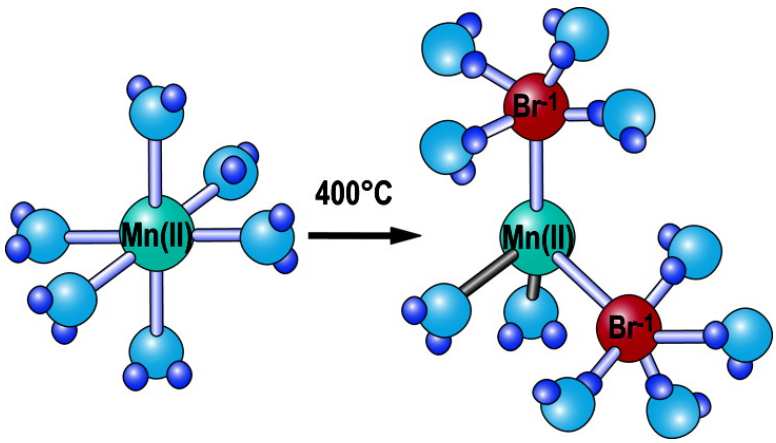

More About This Article

Additional resources and features associated with this article are available within the HTML version:

- Supporting Information
- Links to the 1 articles that cite this article, as of the time of this article download
- Access to high resolution figures
- Links to articles and content related to this article
- Copyright permission to reproduce figures and/or text from this article

View the Full Text HTML

J|A|C|S
ARTICLES
Published on Web 09/17/2005

The Structure of the Homogeneous Oxidation Catalyst, $Mn(II)(Br^{-1})_x$, in Supercritical Water: An X-ray Absorption Fine-Structure Study

Yongsheng Chen,[†] John L. Fulton,*[,†] and Walter Partenheimer*[,‡]

Contribution from the Chemical Sciences Division, Pacific Northwest National Laboratory, Richland, Washington 99352, and Central Research and Development, E. I. DuPont de Nemours & Co. Inc., Experimental Station, Wilmington, Delaware 19880

Received May 25, 2005; E-mail: john.fulton@pnl.gov; delparts@worldnet.att.net

Abstract: Extended X-ray absorption fine structure (EXAFS) and X-ray absorption near edge structure (XANES) spectroscopies were used to probe the first-shell coordination structure about Mn(II) and Br^{-1} ions that exist as contact ion pairs in supercritical water. This work was performed to clarify why solutions of $MnBr_2$ in supercritical water are known to effectively catalyze the aerobic oxidative synthesis of terephthalic acid from *p*-xylene as well as a number of other methylaromatic compounds. The Mn and Br K-edge spectra were collected at the bending magnet beamline (sector 20) at the Advanced Photon Source, Argonne National Laboratory. The first-shell coordination structure about the Mn(II) ion changes from octahedral at ambient conditions to tetrahedral at supercritical conditions. Under supercritical conditions, the measured bond distances of $Mn-OH_2$ and Mn−Br are 2.14 and 2.46 Å, respectively. Direct contact ion pairs form with about 2 Br^{-1} ions present in the first coordination shell of the Mn(II) ion. The structure of dissolved $MnBr_2$, below 1.0 *m*, changes from essentially $[Mn(II)(H_2O)_6]^{+2}$ to $[Mn(II)(H_2O)_2(Br^{-1})_2]$ in supercritical water (scH_2O). When an excess of Br^{-1} ion is added, the bromide coordination number increases and the number of water molecules decreases. The results show that the initial $MnBr_2$ catalyst in scH_2O is tetrahedral with two Mn−Br contact ion pairs. The presence of the acetate anion deactivates the catalyst by formation of insoluble MnO.

Introduction

Terephthalic acid (1,4-dicarboxybenzene), the ninth largest industrial chemical, is the major component in polyester manufacture, and it is currently manufactured by the liquid phase, homogeneous, aerobic oxidation of *p*-xylene in acetic acid solvent using a catalyst consisting of cobalt(II) and manganese(II) acetates with hydrobromic acid. A remarkable advance has been recently reported in which acetic acid is replaced by water as the solvent while giving a product of exceptionally high purity.[1−3] The new chemistry is the continuous conversion of *p*-xylene to terephthalic acid in up to 90% yield via homogeneous reaction in supercritical water (scH_2O, with a critical point of $T_c = 374$ °C, $P_c = 221$ bar) using dioxygen as the primary oxidant and $MnBr_2$ as the catalyst:

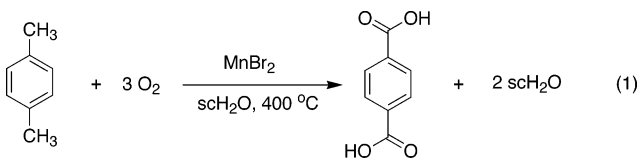

(1)

This new, green chemistry can potentially replace the current less efficient chemical process, which has been in existence for nearly 50 years. What is more, this type of organic oxidation chemistry in supercritical water is applicable to a broad class of similar compounds.[1] However a present limitation in applying this type of chemistry is that the structure and role of the catalytic species is poorly understood. It has been previously predicted, based on the different solvent properties of acetic acid, scH_2O, and non-scH_2O, that the active catalytic species is a contact ion pair wherein the transition metal cation is directly coupled with the counterion.[1] Without detailed structural information about the nature of the catalytic species it is more difficult to understand the underlying mechanism of the reaction which can lead to improvements to the catalyst system. In this article we provide the first detailed structural information about the ion-pair species at reaction conditions.

The significance of this new chemistry with respect to the terephthalic acid synthesis is three-fold: (1) it is more energy efficient,[2] (2) the highly selective scH_2O process eliminates the most problematic impurity 4-carboxybenzaldehyde, and (3) it obviously eliminates problems present in the current process due to the presence of acetic acid. In the existing process

[†] Pacific Northwest National Laboratory.
[‡] E. I. DuPont de Nemours & Co. Inc.

(1) Garcia-Verdugo, E.; Venardou, E.; Thomas, W. B.; Whiston, K.; Partenheimer, W.; Hamley, P. A.; Poliakoff, M. *Adv. Synth. Catal.* **2004**, *346*, 307.
(2) Hamley, P. A.; Ilkenhans, T.; Webster, J. M.; Garcia-Verdugo, E.; Venardou, E.; Clarke, M. J.; Auerbach, R.; Thomas, W. B.; Whiston, K.; Poliakoff, M. *Green Chem.* **2002**, *4*, 235.
(3) Garcia-Verdugo, E.; Fraga-Dubreuil, J.; Hamley, P. A.; Thomas, W. B.; Whiston, K.; Poliakoff, M. *Green Chem.* **2005**, *7*, 294.

10.1021/ja053421v CCC: $30.25

4-carboxybenzaldehyde is present in only a few tenths of a percent but must be removed, at major expense, from the terephthalic acid because of a number of undesirable reactions that occur during the subsequent polymerization of terephthalic acid with ethylene glycol to produce poly(ethylene terephthalate). The significance of the replacement of the acetic acid solvent with scH_2O has many positive aspects. First, roughly 5 g of acetic acid are oxidized, principally to carbon dioxide and carbon monoxide, per 100 g of terephthalic acid that is produced. Second, the water produced in the process, see reaction (rxn) 1, strongly deactivates the Co/Mn/Br catalyst, thereby forcing the use of high concentrations of the more expensive catalyst combination. Finally, because of the deactivation caused by water, the water must be separated from the acetic acid by distillation, another expensive step. An economic analysis of oxidation of *p*-xylene in supercritical water is available.[4]

The successful autoxidation of methylaromatic compounds to carboxylic acids in scH_2O is a very recent accomplishment, and hence much less chemistry is known in scH_2O than in acetic acid/water mixtures.[1,2,5−9] This work will begin to address a number of puzzling observations. Thus far, all evaluated successful catalysts in scH_2O use a bromide/metal ratio of 2/1 mol/mol rather than a 1/1 ratio as used in acetic acid/water mixtures. Typically, metal bromide salts such as $CoBr_2$, $MnBr_2$, and $NiBr_2$ have been used. An attempt to use a 1/1 bromide/metal ratio in scH_2O, by mixing $MnBr_2$ with $Mn(acetate)_2$, produced a very low yield.[7] Acetic acid is used in the current process because it gives high activity and selectivity. In contrast, subcritical water at approximately 200 °C is a very poor solvent[1] for oxidation consistent with the deactivation of the catalytic process by water. Then why is scH_2O an active oxidation solvent? Is there a structural similarity of the catalysts in the active solvents—acetic acid and scH_2O? This work will present the first structural characterization of the manganese/bromide catalyst and suggest answers to the above questions.

X-ray absorption fine structure (XAFS) provides detailed information on the hydration structure about transition metal cations. There are abundant publications in the literature for hydration structures under ambient conditions, whereas only a few are found for supercritical conditions,[10−13] and none yet exists for Mn(II). A general observation is that when the aqueous systems change from ambient to supercritical conditions, it results in a reduction of hydration coordination number and formation of contact ion pairs. Even less attention has been paid to anions, such as Br^{-1}.[14,15] In an earlier study we reported detailed XAFS results of the hydration structure of Mn(II)/bromide mixtures under ambient conditions.[16] In dilute solution, Mn(II) is octahedrally coordinated with six water molecules. As the concentration approaches the saturation limit at 6 *m*, a contact ion pair forms with an average of one bromine in the first coordination shell. Interestingly, EXAFS and XANES results show that the coordination structure retains the octahedral symmetry even with the Mn−Br ion pairing. In this work, the hydration and ion pair structures of Mn(II) and Br^{-1} under supercritical conditions are explored.

Certain terms used by spectrocopists and inorganic chemists will be used interchangeably in this article. Thus "a manganese/bromide contact ion-pair" is synonymous with a "metal/bromide bond". A solvent-separated ion pair has a single solvent molecule between the anion and cation.

Experimental Section

Mn K-edge (6537.7 eV) and Br K-edge (13474 eV) XAFS spectra were collected in transmission mode on a bending magnet beamline (Sector 20) run by the Pacific Northwest Consortium Collaborative Access Team (PNC-CAT) at the Advanced Photon Source, Argonne National Laboratory. The details of the X-ray optics arrangement for these XAFS experiments have been described elsewhere.[16] The solid samples, MnO (Alfa Aesar, 99.5%), Mn_2O_3 (Assay, 98%), and MnO_2 (Alfa Aesar, 99.999%), were ground and prepared on tapes using standard methods. The aqueous $MnBr_2$ solutions used in this study were prepared from manganese(II) bromide tetrahydrate, $MnBr_2{\cdot}4H_2O$, (Aldrich, 98%) and distilled water. This salt is the same used in the oxidative synthesis of terephthalic acid from *p*-xylene.[1,2] Throughout this paper, concentrations are expressed in molality, *m* (mol/kg water). For comparison to the single-salt solution, we examined three mixtures, 0.2 *m* $MnBr_2$ + 0.8 *m* NaBr, 0.2 *m* $MnBr_2$ + 0.03 *m* HBr, and 0.005 *m* $MnBr_2$ + 0.005 *m* $Mn(CH_3COO)_2$. In this case the NaBr (Aldrich, 99.99%), hydrobromic acid (Aldrich, 99.999%), $MnBr_2{\cdot}4H_2O$, and $Mn(CH_3COO)_2{\cdot}4H_2O$ (Aldrich, 99%) were used as received. The solutions used under supercritical conditions were prepared from either aerobic or anaerobic starting solutions. Anaerobic solutions were prepared by purging the distilled, deionized water with nitrogen gas for 2 h prior to use. Each prepared solution was used to fill a Teflon sample bag (25 mL) that was part of a dispensing system to a high-pressure cell. The design of the cell and the dispensing system have been described in detail elsewhere.[17−19] The cell was resistively heated, and the temperature was measured using a three-mode controller (Watlow, series 93) with two platinum resistance temperature detectors (PRTD). The solution sample was injected directly into the cell by a syringe pump (ISCO model 100DX), and the pressure was measured using an electronic transducer (Precise Sensors, Inc., No. D451). For these studies, the transmission path length was 2.5 mm. The high-temperature spectra were acquired by co-adding approximately five, 20-min scans. In the energy range of Mn K-edge XAFS, a single group of three diffraction peaks from the diamond [1 1 0] windows were superimposed over the EXAFS spectra at about 6690, 6820, and 6910 eV. A standard procedure was used to remove those diffraction peaks by subtracting corresponding pure water XAFS spectra at the same temperature and pressure.[18] The Br spectra were corrected in a similar way, followed by removal of multielectron excitations using methods that have been previously described.[15]

The EXAFS data processing has been described in detail in the previous study.[16] In short, the EXAFS oscillations, $\chi(k)$, were extracted

(4) Dunn, J. B.; Savage, P. E. *Green Chem.* **2003**, *5*, 649.
(5) Holliday, R. L.; Jong, B. Y. M.; Kolis, J. W. *J. Supercritical Fluids* **1998**, *12*, 255.
(6) Kim, Y. L.; Kim, J. D.; Lim, J. S.; Lee, Y. W.; Yi, S. C. *Ind., & Engin. Chem. Research* **2002**, *41*, 5576.
(7) Dunn, J. B.; Savage, P. E. *Ind., & Engin. Chem. Research* **2002**, *41*, 4460.
(8) Dunn, J. B.; Urquhart, D. I.; Savage, P. E. *Adv. Synth. Catal.* **2002**, *344*, 385.
(9) Dunn, J. B.; Savage, P. E. *Environ. Sci. Technol.* **2005**, *39*, 5427.
(10) Hoffmann, M. M.; Darab, J. G.; Palmer, B. J.; Fulton, J. L. *J. Phys. Chem. A* **1999**, *103*, 8471.
(11) Mayanovic, R. A.; Jayanetti, S.; Anderson, A. J.; Bassett, W. A.; Chou, I. M. *J. Chem. Phys.* **2003**, *118*, 719.
(12) Fulton, J. L.; Hoffmann, M. M.; Darab, J. G. *Chem. Phys. Lett.* **2000**, *330*, 300.
(13) Seward, T. M.; Henderson, C. M. B.; Charnock, J. M. *Chem. Geol.* **2000**, *167*, 117.
(14) Ferlat, G.; San Miguel, A.; Jal, J. F.; Soetens, J. C.; Bopp, P. A.; Daniel, I.; Guillot, S.; Hazeman, J. L.; Argoud, R. *Phys. Rev. B* **2001**, *6313*.
(15) Wallen, S. L.; Palmer, B. J.; Pfund, D. M.; Fulton, J. L.; Newville, M.; Ma, Y. J.; Stern, E. A. *J. Phys. Chem. A* **1997**, *101*, 9632.
(16) Chen, Y.; Fulton, J. L.; Partenheimer, W. *J. Solution Chem.* **2005**, *34*, 993.
(17) Hoffmann, M. M.; Darab, J. G.; Heald, S. M.; Yonker, C. R.; Fulton, J. L. *Chem. Geol.* **2000**, *167*, 89.
(18) Fulton, J. L.; Pfund, D. M.; Ma, Y. J. *Rev. Sci. Instrum.* **1996**, *67*, 3364.
(19) Fulton, J. L.; Chen, Y.; Heald, S. M.; Balasubramanian, M. *Rev. Sci. Instrum.* **2004**, *75*, 5228.

from the experimentally measured absorption coefficient using an automated background subtraction method (AUTOBK) developed by Newville et al.[20] The EXAFS relationship is given by

$$\chi(k) = \sum_i \frac{F_i(k) S_0^2 N_i}{kR_i^2} \exp(-2k^2\sigma_i^2) \exp\left[\frac{-2R_i}{\lambda(k)}\right] \sin\left(2kR_i + \delta_i(k) - \frac{4}{3}k^3 C_{3,i}\right)$$

where the sum is over all possible single scattering paths and for all the significant multiple scattering paths. k is the wavenumber of the ejected photoelectron and equal to $\sqrt{2m_e(E-E_0)/\hbar^2}$ with E_0 being the absorption edge energy. R_i, N_i, and σ_i^2 are the path length, the number of equivalent paths, and the Debye−Waller factor for a group of equivalent scattering paths. For single scattering paths, R and N equal the distance and the coordination number of the scattering atoms, respectively. σ_i^2 represents the mean-square variation in R_i due to both static and thermal disorder. $F_i(k)$, $\delta_i(k)$, and $\lambda(k)$ are the amplitude, phase, and mean-free-path factors, respectively, that are derived from theoretical standards calculated by FEFF8.[21] S_0^2 is the core-hole or amplitude-reduction factor, which was set to 0.72 (±20%) based upon three solid standards.[16] The final parameter is $C_{3,i}$, the anharmonicity of the pair-distribution. In this work, the Mn $\chi(k)$ data were weighted by k^2, and windowed between $2.0 < k < 12.0$ Å^{-1} using a Hanning window with $dk = 1.0$ Å^{-1}. For the Br $\chi(k)$ data, the k range was $1.75 < k < 12.0$ Å^{-1}. Fitting parameters and their definitions are the same as in the previous study.[16] The fits were to both the real and imaginary parts of $\tilde{\chi}(R)$ in the region of $1.0 < R < 3.0$ Å. Quality of fits was evaluated using the criteria defined in FEFFIT, the automated software for fitting the structural parameters.[22,23]

Results and Discussion

EXAFS Spectra. At ambient conditions, when $MnBr_2$ is present at concentrations below about 1 *m*, the Mn(II) is hydrated with six water molecules in an octahedral arrangement.[16] This structure changes dramatically under supercritical conditions (the critical point corresponds to 374 °C and 220 bar) as shown qualitatively in Figure 1 which presents the k^2-weighted $|\tilde{\chi}(R)|$ plots for 0.2 *m* $MnBr_2$ solutions at 25 °C (1 bar), 325 °C (140 bar), and 400 °C (310 bar). There are two peaks located at about 1.7 and 2.3 Å, corresponding to first-shell oxygen and bromine, respectively. (The distances are taken directly from the plot before phase correction, whereas the true distances will be reported from the fitting.) Qualitatively, the amount of oxygen (from water) is almost halved when the temperature is raised to 325 °C, a subcritical point, and the amount of bromine increases in the first shell. When the system is under supercritical conditions at 400 °C, the number of oxygens is further reduced and more bromine is present. These observations are qualitatively similar to the UV−vis spectroscopic studies of the association behavior of $MnCl_2$ in water up to 300 °C.[24]

The quantitative coordination structural information reported in Table 1 is obtained by fitting the experimental data to FEFF8 theoretical standards.[22,23] As the temperature increases to the supercritical state, the coordination number about Mn(II) of water molecules decreases from 6 to about 2, while those of bromine increase from 0 at 25 °C to about 2 for both 325 and 400 °C. The EXAFS results thus clearly suggest that the geometry of the ligands changes from an octahedral to a tetrahedral structure (see further discussion in XANES and Preedge Spectra section). The majority of the coordination changes from octahedral to tetrahedral has already occurred by 325 °C. To increase the degree of ion pairing, NaBr was added as a second salt to provide an excess of Br^{-1}. Since Na(I) is only monovalent and the ion radius is much larger than that of Mn(II), the propensity for ion pairing is significantly less for NaBr than that for $MnBr_2$. When excess Br^{-1} is present, as is shown in Table 1 for the mixture of 0.2 *m* $MnBr_2$ and 0.8 *m* NaBr at 400 °C, the average Br^{-1} coordination number has now increased to about 3.4 and the total coordination number is approximately 4 showing that the tetrahedral structure still persists. Another factor affecting ion pairing under supercritical conditions is the degree of hydrolysis of the cation to form $[Mn(II)(H_2O)_{2-x}(OH^-)_x\ (Br^{-1})_2]$ species. For this reason one condition was also explored that contained 0.03 *m* HBr with the 0.2 *m* $MnBr_2$ generating a starting ambient pH of 1.5. This

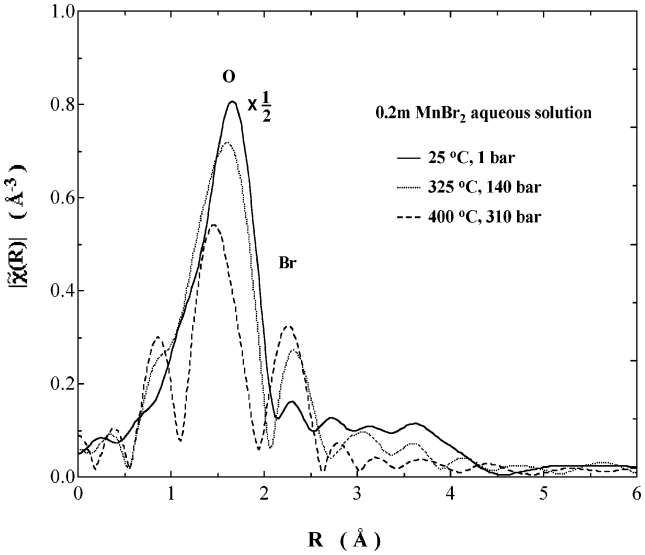

Figure 1. The k^2-weighted $|\tilde{\chi}(R)|$ plots for 0.2 *m* $MnBr_2$ solutions at 25 °C (solid), 325 °C (dotted), and 400 °C (dashed). The intensity for the solution at 25 °C is halved to fit the figure.

Table 1. Results of the EXAFS Analysis of the Mn(II) First Shell Structure in Aqueous Solutions at Different Temperatures (corresponding pressures are listed in the text)[a]

system	temp (°C)	scatterer	*N*	*R* (Å)	σ^2 (×10^{-3} Å^2)	$\mathcal{R}$[b]
0.2 *m* $MnBr_2$	25	O	6.0 (0.3)	2.17 (1)	6.2 (0.8)	0.02
		Br	0	-	-	
0.2 *m* $MnBr_2$	325	O	2.8 (0.3)	2.15 (1)	7.6 (1.9)	0.011
		Br	2.1 (1.1)	2.52 (2)	15.5 (5.3)	
0.2 *m* $MnBr_2$	400	O	1.7 (1.3)	2.11 (8)	11.3 (16.4)	0.24
		Br	1.9 (2.4)	2.46 (4)	12.0 (10.9)	
0.2 *m* $MnBr_2$ +	400	O	1.3 (1.4)	2.18 (6)	11.7 (29.2)	0.25
0.03 *m* HBr		Br	2.5 (2.9)	2.46 (3)	13.4 (11.3)	
0.2 *m* $MnBr_2$ +	400	O	0.9 (0.4)	2.10 (4)	5.1 (7.6)	0.076
0.8 *m* NaBr		Br	3.4 (1.6)	2.47 (2)	14.3 (4.4)	

[a] *N*, *R*, and σ^2 are the coordination number, bond distance, and the Debye−Waller factor, respectively. The concentrations are expressed in molality. k range is from 2 to 12 Å^{-1}, and k^2-weighting is applied [b] Goodness of fit defined by a scaled sum of squares as described in FEFFIT.

(20) Newville, M.; Livins, P.; Yacoby, Y.; Rehr, J. J.; Stern, E. A. *Phys. Rev. B* **1993**, *47*, 14126.
(21) Zabinsky, S. I.; Rehr, J. J.; Ankudinov, A.; Albers, R. C.; Eller, M. J. *Phys. Rev. B* **1995**, *52*, 2995.
(22) Stern, E. A.; Newville, M.; Ravel, B.; Yacoby, Y.; Haskel, D. *Physica B* **1995**, *209*, 117.
(23) Newville, M.; Ravel, B.; Haskel, D.; Rehr, J. J.; Stern, E. A.; Yacoby, Y. *Physica B* **1995**, *209*, 154.
(24) Suleimenov, O. M.; Seward, T. M. *Chem. Geol.* **2000**, *167*, 177.

Table 2. Results of the Global Model Fit to Both Mn(II) and Br^{-1} EXAFS Measurements in 0.2 and 0.4 *m* Aqueous $MnBr_2$ Solutions at 400 °C[a]

system	absorbing center	scatterer	*N*	*R* (Å)	σ^2 ($\times 10^{-3}$ Å^2)	$\mathscr{R}$[b]
0.2 *m* $MnBr_2$	Mn	O	2.3 (0.8)	2.13 (2)	14.3 (8.4)	0.21
		Br	1.6 (0.4)	2.46 (1)	12.3 (2.7)	
	Br	O	5.3 (3.2)	3.27 (4)	88.8 (30.4)	0.083
		Mn	0.8 (0.2)	2.46 (1)	12.3 (2.7)	
0.4 *m* $MnBr_2$	Mn	O	1.8 (0.3)	2.14 (1)	5.1 (2.8)	0.046
		Br	1.6 (0.4)	2.46 (1)	11.9 (2.3)	
	Br	O	4.1 (2.0)	3.27 (3)	74.0 (23.6)	0.11
		Mn	0.8 (0.2)	2.46 (1)	11.9 (2.3)	

[a] *N*, *R*, and σ^2 are the coordination number, bond distance, and the Debye−Waller factor, respectively. The concentrations are expressed in molality. *k* range is from 2 to 12 Å^{-1}, and k^2-weighting is applied. [b] Goodness of fit defined by a scaled sum of squares as described in FEFFIT.

would lower the pH to shift the equilibria away from the hydrolyzed species. The first shell coordination numbers and structures are not significantly altered indicating that the hydrolyzed species do not represent a significant fraction of the total Mn(II) speciation at these concentrations.

For the two different systems listed in Table 2, *both* Mn and Br *K*-edge spectra were acquired for each system. In this way the measurement uncertainties can be greatly reduced by applying a global model fit to both Mn(II) and Br^{-1} $\chi(k)$ data sets. Both data sets share the common parameters of the coordination number of Br around the Mn(II) (or two times the coordination number of Mn around Br), the Mn−Br bond distance, and its Debye−Waller factor. The k^2-weighted $\chi(k)$ and $|\tilde{\chi}(R)|$ plots of both the fits and the experimental data for 0.4 *m* aqueous $MnBr_2$ solutions at 400 °C are shown in Figure 2. In the $|\tilde{\chi}(R)|$ plots the positional ordering of the Br, O and Mn atoms about their respective ions are shown and a very qualitative indication of the relative coordination numbers are indicated by the relative peak heights. The resulting global fit parameters for both 0.2 and 0.4 *m* aqueous $MnBr_2$ solutions at 400 °C are presented in Table 2. Comparison of the fit parameters listed in Tables 1 and 2 for 0.2 *m* $MnBr_2$ solution at 400 °C shows a significant reduction in the uncertainties associated with each variable. As shown in Table 2, the structural parameters for the 0.2 and 0.4 *m* solutions are very similar. A large source of uncertainty associated with the fitted coordination number comes from the estimation of the core hole factor, S_0^2 (see EXAFS expression). Hence, if we assume that Mn is octahedrally coordinated (N is *exactly* 6.0) for the well-characterized 0.2 *m* $MnBr_2$ solution in ambient conditions we can eliminate this source of uncertainty. Then the total coordination numbers around Mn for the 0.2 and 0.4 *m* $MnBr_2$ solutions at 400 °C will be 3.9 ± 1.2 and 3.4 ± 0.7 (see Table 1). Both ranges include the preferred value of 4 for tetrahedral structure. The coordination number for Br^{-1} about Mn(II) is less than two perhaps suggesting that there is a small percentage of singly paired Mn−Br in equilibria with the fully ion paired species, i.e., $[Mn(H_2O)_2Br_2] + H_2O \leftrightarrow [Mn(H_2O)_3Br]^+ + Br^{-1}$.

The best estimate of the Mn−water distance under supercritical conditions is provided by the 0.4 *m* $MnBr_2$ solutions where we find a distance of 2.14 ± 0.01 Å. This is only slightly smaller than the value at 25 °C of 2.17 ± 0.01 Å. However, the model fit at high temperature does not include the anharmonicity of the pair distribution function ($C_{3,i}$) because the EXAFS amplitudes at higher *k* are too low (Mn−O coordination number is lower) to accurately evaluate its value.[16] Hence, no significance can be attached to the small decrease in the Mn−O bond distance.

XANES and Preedge Spectra. The XANES and preedge spectra for the 0.2 *m* $MnBr_2$ aqueous solutions at 25, 325, and 400 °C shown in Figure 3 provide complementary information to EXAFS measurements from changes in the bound-state electron transitions. As shown by the previous study,[16] there are two main features in the Mn(II) preedge spectra: a small preedge peak at about 4539.5 eV and a shoulder on the edge corresponding to the 1s → 3d and 1s → 4p excitations, respectively. The 1s → 3d transition is formally forbidden for octahedral symmetries, but due to p−d hybridization a weaker quadrupolar transition is allowed.[25] For tetrahedral symmetry the more intense dipole transition is allowed. A comprehensive review by Farges of 31 different Mn compounds reveals that this 1s → 3d preedge feature provides an accurate measurement of the Mn site symmetry and oxidation state.[25] For three oxidation states, Mn(II), Mn(III), and Mn(IV), the centroid of the preedge peak shifts consistently by a total of 1 eV toward higher energy with higher oxidation state. The preedge peak intensity changes with both the symmetry and oxidation state but much more so with symmetry. Quantitatively, an increased distortion at the octahedral site about Mn(II) can lead to an increase of the peak intensity by up to 20%, while a symmetry change from an undistorted octahedral structure to a tetrahedral structure can result in 2−3 times increase of the peak intensity.[25] Furthermore, our previous study shows that at ambient conditions this preedge peak intensity does not change when bromide replaces oxygen (from water) in an octahedral structure.[16] Hence, in this study, we can use this preedge feature to conclusively determine the site symmetry of Mn. In Figure 3 we see that the band position does not shift, indicating that no change in oxidation state occurs. We also see that the band intensity for 1s → 3d transition for 0.2 *m* $MnBr_2$ increases by a factor of about 3 for all solutions at 400 °C. This indicates conclusively that the Mn(II) is at a tetrahedral site. This result confirms the above EXAFS measurements.

In Figure 3, the spectra of two mixed salt solutions, 0.2 *m* $MnBr_2$ + 0.03 *m* HBr and 0.2 *m* $MnBr_2$ + 0.8 *m* NaBr, are also presented for comparison. The 1s → 3d band intensities for the two mixtures, having low pH (with 0.03 *m* HBr) and significant excess of Br^{-1} (with 0.8 *m* NaBr), are almost the same as that for pure 0.2 *m* $MnBr_2$ solution at the same temperature. This observation also confirms the above EXAFS analysis that the tetrahedral symmetry persists under varying Br^{-1} concentration. This analysis also confirms that the 1s → 3d transition is sensitive to symmetry change but not to first shell atom types.

Our earlier study of ambient $MnBr_2$ solution showed that the 1s → 4p band at 6545 eV is associated with the formation of ion pairs.[16] There are two kinds of ion pairs, direct-contact ion pairs (Mn−Br) and solvent-shared ion pairs (Mn···H_2O···Br). Under supercritical conditions, the dielectric constant of water dramatically decreases; thus, the ionic interaction between cations and anions increases significantly. The presence of the solvent-shared ion pairs should be much less prevalent than that at ambient conditions. This 1s → 4p band grows to a maximum for the mixture of 0.2 *m* $MnBr_2$ + 0.8 *m* NaBr at 400 °C. The

(25) Farges, F. *Phys. Rev. B* **2005**, *71*, 155109.

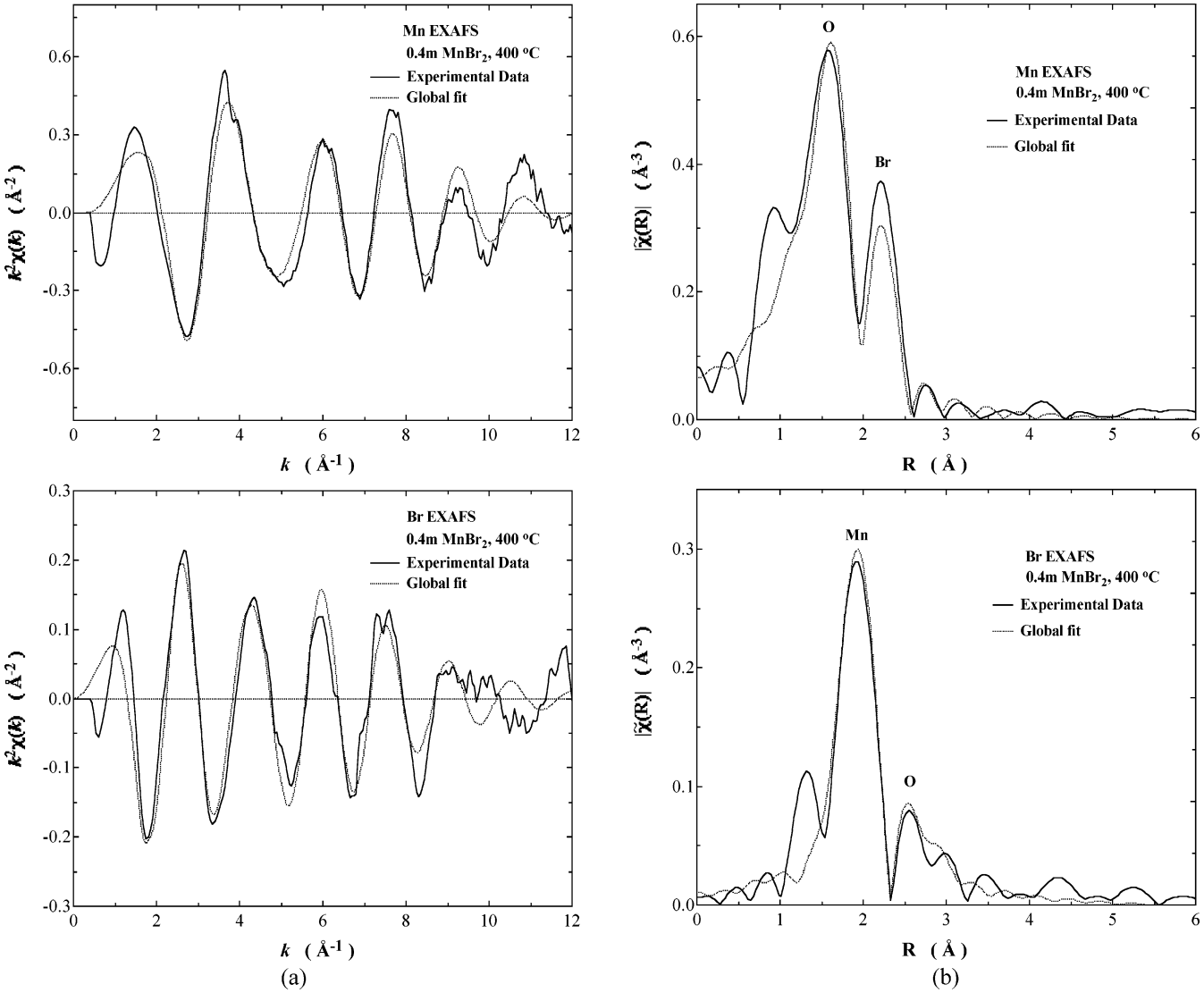

Figure 2. The k^2-weighted (a) $\chi(k)$ and (b) $|\tilde{\chi}(R)|$ plots for 0.4 *m* aqueous $MnBr_2$ solutions at 400 °C at both the Mn and Br K-edges. The solid line shows the experimental data and the dotted line shows the global model fit to both data sets using FEFF calculations and the parameters listed in Table 2.

band intensities for 0.2 *m* $MnBr_2$ and for the mixture of 0.2 *m* $MnBr_2$ + 0.03 *m* HBr at 400 °C are nearly identical, since there is only slight excess of Br^{-1} in the mixture. They are between the intensities of 0.2 *m* $MnBr_2$ at lower temperatures and the same system with added Br^{-1}. The result shows that the 1s → 4p band is sensitive to compositional changes, and in this case, the degree of ion pairing with Br^{-1}. This XANES result again suggests that the degree of Mn(II) hydrolysis is minor at these concentrations because by exchanging the Br^{-1} with OH^- or by replacing a H_2O with OH^- we would expect to see change in the intensity of the 1s → 4p feature, which is not observed.

Overall, these results show that the 1s → 3d transition is sensitive to the symmetry change but not to the compositional change. On the other hand, we see that the 1s → 4p, at approximately 6545 eV, undergoes a slight increase in the intensity when the degree of ion pairing with Br^{-1} increases for solution containing 0.8 *m* NaBr. This sensitivity of the preedge region to both the symmetry and coordination number is an important feature for the spectral analysis in the following section for which we examine very dilute solutions of $MnBr_2$ where high-quality EXAFS spectra are not available.

Catalyst Structure. $MnBr_2$ is a very effective catalyst for selective, homogeneous, aerobic oxidation of organic molecules in supercritical water and potentially the best catalyst for terephthalic acid synthesis. The working catalyst is used at a much lower concentration of about 0.01 *m*. For such dilute systems, EXAFS measurements are difficult because of weak signal at higher *k*. Fortunately, the XANES spectra provide good spectral quality. Figure 4 shows the XANES and preedge spectra at the Mn K-edge for different aqueous $MnBr_2$ solutions having concentrations from 0.01 to 0.4 *m* under supercritical conditions at 400 °C. All four spectra are almost identical. The 1s → 3d transition has the same band intensities, suggesting tetrahedral symmetry for all four solutions. The 1s → 4p band intensities are also the same, suggesting little change in the number of $Mn(II)-Br^{-1}$ ion pairs in the dilute system. This result concludes that for the initial catalyst, Mn(II) has tetrahedral symmetry and most of the Mn(II) and Br^{-1} are in the form of contact ion pairs with a $Mn(II)/Br^{-1}$ ratio of 1/2, as observed in 0.4 *m* solution.

Catalysis Mechanisms. Starting from the known structure of the catalyst it is now possible to further develop our understanding of the catalyst mechanism for aerobic oxidation

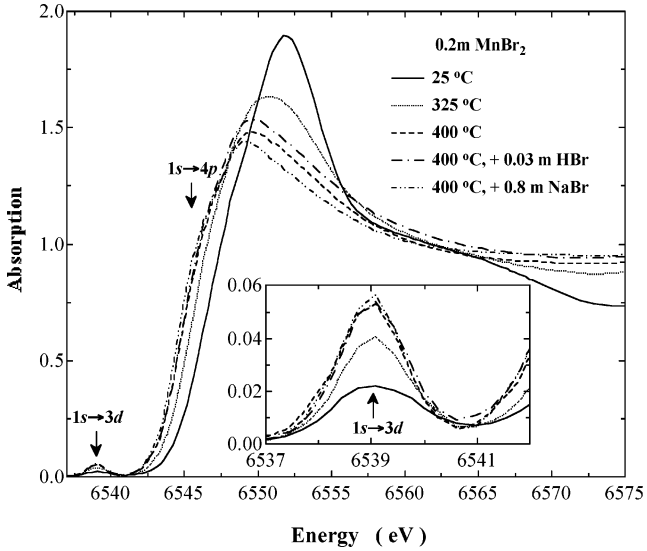

Figure 3. XANES and preedge spectra at the Mn K-edge for a 0.2 *m* $MnBr_2$ aqueous solution at different temperatures: 25 °C (solid), 325 °C (dotted), and 400 °C (dashed). For comparison, the spectra of two mixture solutions at 400 °C are also presented, 0.2 *m* $MnBr_2$ + 0.03 *m* HBr (dash dotted) and 0.2 *m* $MnBr_2$ + 0.8 *m* NaBr (dash double dotted). The 1*s*→3*d* transition is shown in detail in the inset. All spectra are scaled to a common edge-height and were measured in transmission mode.

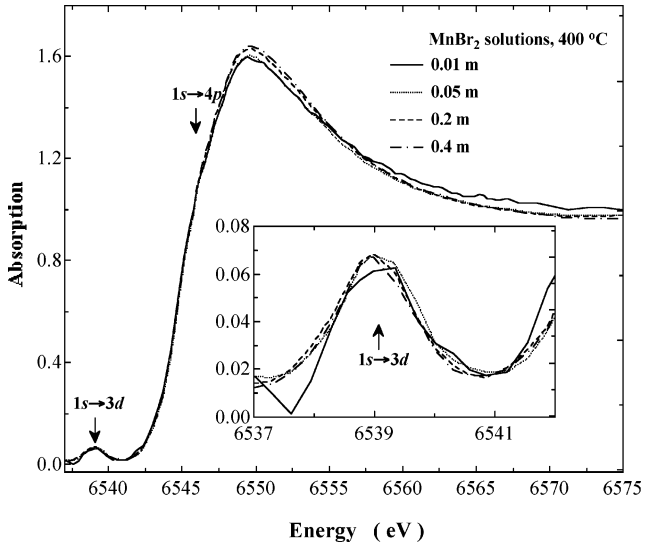

Figure 4. Comparison of XANES and preedge spectra at the Mn K-edge for different concentrations of $MnBr_2$ aqueous solutions under supercritical conditions, 0.01 *m* (solid), 0.05 *m* (dotted), 0.2 *m* (dashed) and 0.4 *m* (dot dashed). The 1*s* → 3*d* transition is shown in detail in the inset. All spectra are scaled to a common edge-height and were measured in transmission mode.

of hydrocarbons. The reaction products from oxidation in scH_2O are the same as those in acetic acid−water mixtures, where the latter reactions are known to proceed via autoxidation.[1,2] Hence, we shall assume the same mechanism applies to scH_2O. Autoxidation is defined as the reaction of dioxygen with the hydrocarbon to produce oxygenates via a free radical chain mechanism. This mechanism has been intensely studied [26] and the metal/bromide-catalyzed oxidation has been reviewed.[27−29] Of the 30 different catalysts reported, the most common catalysts contain Co(II) acetate or mixtures of Co(II) and Mn(II) acetates.[27] The most important solvent is acetic acid, because it produces high activity and is the most oxidatively resistant. A detailed discussion of the mechanism is beyond the scope of this paper and will be limited to a discussion of how the benzylic radical is generated.

The free radical chain mechanism involves an initiation step to generate the highly reactive benzylic radical:

$$PhCH_3 + X \rightarrow PhCH_2^{\bullet} + \text{products} \qquad (2)$$

The benzylic radical then reacts rapidly with dioxgen in the propagation step to produce the peroxy radical which reacts with another mole of the methylaromatic compound to generate the peroxide.

$$2PhCH_3^{\bullet} + O_2 \rightarrow PhCH_2^{\bullet} + PhCH_2OO^{\bullet} \qquad (3)$$

$$PhCH_2OO^{\bullet} + PhCH_3 \rightarrow PhCH_2OOH + PhCH_2^{\bullet} \qquad (4)$$

One of the critical reactions which is responsible for the characteristic properties of metal/bromide catalysts involves the oxidation of the metal and subsequent reduction of the bromide anion. In the mechanism below we show the reaction of the bromide anion occurring within the coordination sphere of the metal:

$$Mn(II) + 2Br^- \xrightarrow[400\ ^\circ C]{(5)} [Mn(II)(H_2O)_2(Br^-)_2] \xrightarrow[\text{oxidant}]{(6),\ -H^+}$$

$$[Mn(III)(H_2O)(OH^-)(Br^-)_2] \xrightarrow{(7)} [Mn(II)(H_2O)(OH^-)(Br^-)(Br^{\bullet})]$$

Upon heating to supercritical conditions, the ion-pair species forms according to rxn 5. The EXAFS results show that a high percentage of the Mn(II) initially exists in the doubly contact ion-pair state so that the oxidation step, rxn 6, likely occurs with this species. The oxidant in rxn 6 is typically a peroxy radical, a peroxide, or a peroxyacid. In supercritical water, charge-neutral ion-pair structures are strongly favored. Hence, after oxidation of the Mn(II) to Mn(III) there is need to retain a charge neutral complex. This is likely achieved by simultaneous oxidation and hydrolysis shown in rxn 6. Hydrolysis is thermodynamically favored for higher oxidation states of the metal; hence, this provides a driving force for rxn 6. The bromine radical, $Br^{\bullet}$, generated in rxn 7, rapidly and selectively generates the benzylic radicals (much more rapidly than Co(III) or Mn(III)).[30,31] In acetic acid, it is thought that the critical $Br^{\bullet}$ species is either the bromine atom coordinated to the metal[30−43] or the formation of $HBr_2^{\bullet}$ radical.[44,45] The latter

(26) Weiner, H.; Trovarelli, A.; Finke, R. G. *J. Mol. Catal. A-Chem.* **2003**, *191*, 217.
(27) Partenheimer, W. *Catal. Today* **1995**, *23*, 69.
(28) Suresh, A. K.; Sharma, M. M.; Sridhar, T. *Ind., & Engin. Chem. Research* **2000**, *39*, 3958.
(29) Fischer, R. W.; Roehrscheid, F. In *Applied Homogeneous Catalysis with Organometallic Compounds*; 2nd ed.; Cornils, B., Herrmann, W. A., Eds.; Wiley-VCH Verlag GmbH, 2002; Vol. 1; p 443.
(30) Partenheimer, W.; Gipe, R. K. *ACS Symposium Series* **1993**, *523*, 81.
(31) Partenheimer, W. A Chemical Model for the Amoco 'MC' Oxygenation Process to Produce Terephthalic Acid. In *Catalysis of Organic Reactions*; Blackburn, D. W., Ed.; Marcel Dekker: 1990.
(32) Bukharkina, T. V.; Gavrilenko, N. D.; Digurov, N. G.; Knyazeva, N. A. *Kinet. Catal.* **1978**, *19*, 402.
(33) Kamiya, Y. *Tetrahedron* **1966**, *22*, 2029.
(34) Kamiya, Y. *J. Catal.* **1974**, *33*, 480.
(35) Kamiya, Y.; Nakajima, T.; Sakoda, K. *Bull. Chem. Soc. Jpn.* **1966**, *39*, 2211.
(36) Sakota, K.; Kamiya, Y.; Ohta, N. *Bull. Chem. Soc. Jpn.* **1968**, *41*, 641.
(37) Batygina, N. A.; Bukharkina, T. V.; Digurov, N. G. *Kinet. Catal.* **1981**, *22*, 920.
(38) Digurov, N. G.; Gavrilenko, N. D.; Bukharkina, T. V.; Enyukova, E. S. *Kinet. Catal.* **1978**, *19*, 105.
(39) Shcherbina, F. F.; Belous, N. P. *Kinet. Catal.* **1983**, *24*, 416.

is easily achievable since there are two bromine species in the coordination sphere:

$$[Mn(II)(H_2O)(OH^-)(Br^-)(Br^\bullet)] \xrightarrow{(8),\ +H_2O} [Mn(II)(H_2O)_2(OH^-)(Br_2^{\bullet -})]$$

Assuming the necessity of charge-neutrality, the $(Br_2^\bullet)^-$ radical will remain bonded to the metal, and this complex will be the active species X in rxn 2. The model is consistent with the experimental observations of low steady-state concentrations of Co(III) and Mn(III) during metal/bromide-catalyzed oxidations in acetic acid and their resultant increase in selectivity due to a decrease in decarboxylation reactions.[31]

In the XANES region the location of the absorption edge is a sensitive indicator of the oxidation state. A higher oxidation state for Mn would result in a 2−3 eV shift to *higher* energy. As we see in Figure 3 the edge position has an apparent shift to lower energy primarily because of the superposition of the 1s → 4p transition immediately prior to the continuum transition. It is unlikely then that the position of the continuum transition at approximately 6547 eV changes under scH_2O conditions. The invariance of the position of the 1s → 3d transition is also an indication that the vast majority of the Mn remains in the Mn-(II) state. On the other hand, for the condition of this study, the O_2/Mn ratio was only 0.1 so oxidative potential under actual reaction conditions may not have been achieved.

Catalyst Structure in the Presence of Acetate. Historically the most successful oxidations in acetic acid use mixed metal/acetate/bromide catalysts at a 1/1 bromide/metals ratio. In fact, in acetic acid, the acetate concentration is known to affect the activity and selectivity in metal/bromide-catalyzed reactions.[27] The report that $MnBr_2$ was an active catalyst (54% yield of terephthalic acid from *p*-xylene) but an equimolal mixture of $MnBr_2$ and $Mn(acetate)_2$ exhibited very poor activity (0.4% yield)[7] was therefore puzzling to us. For this reason we explored the structure of a 1/1 bromide/metal ratio in scH_2O by using an equimolal mixture of $MnBr_2$ and $Mn(acetate)_2$. The XANES and preedge spectra of 0.005 *m* $MnBr_2$ + 0.005 *m* $Mn(acetate)_2$ mixtures at 400 °C are shown in Figure 5, together with those for 0.01 *m* $MnBr_2$ and solid MnO. In this case deoxygenated water was used to prepare this solution to avoid possible oxidative degradation of the acetate as well as the oxidation of the Mn(II) to Mn(III) or Mn(IV) during these static measurements. For solid MnO, the first-shell oxygen atoms have a perfect octahedral coordination structure around Mn(II); hence, the spectrum displays a very weak preedge peak due to the 1s → 3d transition (see the inset in Figure 5). As previously noted, the 1s → 3d transition peak for 0.01 *m* $MnBr_2$, which possesses a tetrahedral symmetry, is much larger, about 3−4 times that of MnO. The 0.005 *m* $MnBr_2$ + 0.005 *m* $Mn(acetate)_2$ mixture at 400 °C has a nearly identical XANES spectrum to that of solid MnO. Further, we found that there was significant increase in the absorption edge height, indicating a significant percentage of a solid MnO phase in equilibrium with the liquid.

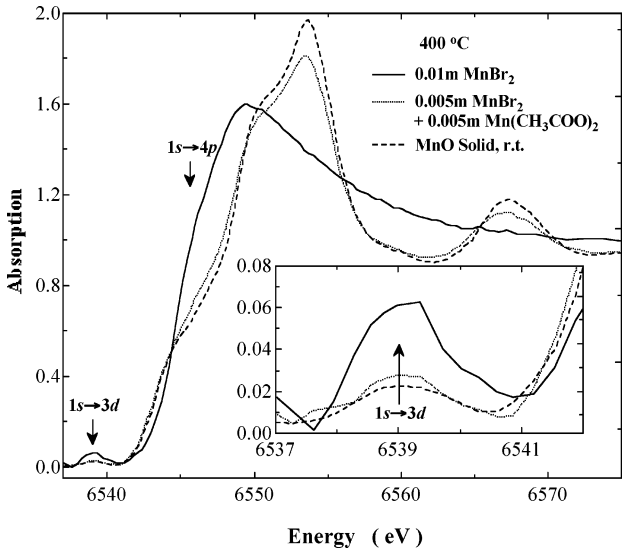

Figure 5. XANES and preedge spectra at the Mn K-edge for 0.01 *m* $MnBr_2$ solution (solid), MnO (dashed), and mixture of 0.005 *m* $MnBr_2$ + 0.005 *m* $Mn(CH_3COO)_2$ in deoxygenated water (dotted). The 1*s* → 3*d* transition is shown in detail in the inset. All spectra are scaled to a common edge-height and were measured in transmission mode.

Thus, a particularly important and surprising observation in this work is that a mixture of $MnBr_2$ and $Mn(acetate)_2$ results in formation of insoluble MnO in scH_2O. The poor catalytic activity of this mixture is *not* due to inherent catalytic characteristics but rather due to precipitation of the catalyst and loss of soluble Mn(II) species. No other oxides, such as Mn_2O_3 or MnO_2, are detected in our experiment, as shown in Figure S1 in the Supporting Information. This result is similar to the precipitation of catalyst observed in acetic acid/water mixtures due to formation of MnO_2 or M(pyromellitate)$_2$ (M = Co(II), Mn(II)) [27] and in scH_2O the formation of MnO_2.[2] The difference is probably due to the different reaction conditions.

The reaction in scH_2O can be formally written as:

$$Mn(II)(CH_2COO)_2 + H_2O \rightarrow Mn(II)O\downarrow + 2\ CH_3COOH \quad (9)$$

The conversion to MnO can best be explained by reviewing the thermodynamic equilibrium of all possible Mn species under supercritical conditions. Such analysis must include effects of the oxidation/reduction potential as well as the solution pH. A very concise representation of this multidimensional thermodynamic space can be summarized in a potential-pH diagram or a Pourbaix diagram. Such a map is not available for Mn compounds under hydrothermal conditions, but extensive maps exist for Ni, Cr, and Fe, and the trends for all of these transition metals are similar.[46−48] To summarize, the stability region for various metal oxide species exists only at pH's above approximately 8 and under oxidizing conditions at ambient conditions. However, at temperatures above 300 °C, this region of stability for the metal oxide species encompasses a much larger area extending down to a much lower pH of about 5. The reason for the precipitation at 400 °C is then that the $MnBr_2$ + $Mn(acetate)_2$ solution has a higher pH. This is illustrated in Table 3 where the pH of the appropriate solutions *at room*

(40) Dugmore, G. M.; Powels, G. J.; Zeelie, B. *J. Mol. Catal. A-Chem.* **1995**, *99*, 1.
(41) Galstyan, A. G.; Tyupalo, N. F. *Petro. Chem.* **2002**, *42*, 314.
(42) Gerber, T. I. A.; Wiechers, A.; Noah, A. T.; Zeelie, B. *S. Afr. J. Chem.-S. Afr. T.* **1998**, *51*, 178.
(43) Hirano, M. S.; Morimoto, T. S. *Bull. Chem. Soc. Jpn.* **1989**, *62*, 4069.
(44) Jiao, X. D.; Metelski, P. D.; Espenson, J. H. *Inorg. Chem.* **2001**, *40*, 3228.
(45) Metelski, P. D.; Espenson, J. H. *J. Phys. Chem. A* **2001**, *105*, 5881.
(46) Beverskog, B.; Puigdomenech, I. *Corros. Sci.* **1996**, *38*, 2121.
(47) Beverskog, B.; Puigdomenech, I. *Corros. Sci.* **1997**, *39*, 969.
(48) Beverskog, B.; Puigdomenech, I. *Corros. Sci.* **1997**, *39*, 43.

Table 3. pH Values of Different Solutions at Room Temperature (air saturated)

solution	pH
0.2 *m* $MnBr_2$	3.7
0.2 *m* $Mn(CH_3COO)_2$	6.9
0.05 *m* $MnBr_2$ + 0.05 *m* $Mn(CH_3COO)_2$	6.4
0.01 *m* $MnBr_2$	5.0
0.01 *m* $Mn(CH_3COO)_2$	6.0
0.005 *m* $MnBr_2$ + 0.005 *m* $Mn(CH_3COO)_2$	6.0

temperature are compared. There is a decrease in pH when $MnBr_2$ is added to water due to the hydrolysis of the Mn(II) and a slight decrease in pH when Mn(acetate)$_2$ is added due to the protonation of acetate anion which is an anion of a weak acid. We assume that the same trends in pH observed at room temperature are also observed in scH_2O explaining why MnO precipitation occurs.

Catalyst Structure−Reactivity in Different Solvents. We will present a simple model relating catalytic activity with the structure of $MnBr_2$ in different solvents and then provide examples of its validity. This model is given in rxns 10−14 where only the ligands necessary for the mechanism are shown:

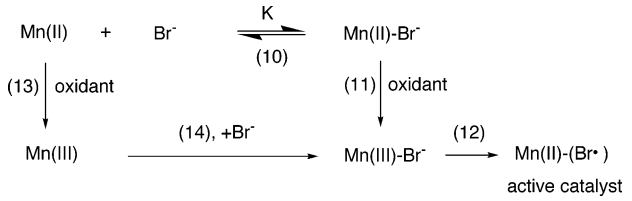

When the equilibrium constant, *K*, in rxn 10 in a given solvent, such as in scH_2O, is sufficiently large, then most of the dissolved Mn(II) will consist of metal/bromide coordination compounds. The generation of the active catalytic species is then via the oxidation of the metal/bromide complex, rxn 11, followed by intramolecular electron transfer to give the active catalytic species via rxn 12. However in ambient water *K* is very small so that formation of the active catalytic species proceeds through the alternate sequence rxn 13 → rxn 14 → rxn 12. The generation of the active catalyst species will be faster via rxns 11, 12 rather than 13, 14, 12 because one additional, slow reaction, rxn 14, is present in the latter. This additional reaction would be expected to be especially slow because the ligand exchange with bromide with Mn(III) is considerably slower than that of Mn(II).[49] For this overall reaction sequence we assume that reactions 11 and 13 are of comparable rates at the same temperature and that the relative activation energies for all reactions stay about the same between ambient and supercritical temperatures. Overall, as the equilibrium constant, *K*, increases, the steady-state concentration of metal/bromide species increases, which results in increasing catalytic activity.

We will now give three examples, which are consistent with the above model. Table 4 gives the relationship between catalytic activity and the degree of metal/bromide species as a function of water concentration in acetic acid. Acetic acid is the solvent currently used in commercial terephthalic acid manufacture. As the amount of metal/bromide species, i.e., contact ion pairs, decreases, there is a concomitant decrease in activity. Thus, the value of *K* increases with an increase in the catalytic activity. The dielectric constant increases from 6.2 to 17 as the rate decreases from 4.8 to 1.2 cm^3 O_2/min. As the dielectric constant decreases, the electrostatic interactions between Co(II) and Mn(II) and Br^{-1} are expected to increase, leading to an increase in *K* in rxn 10.

In this work we have shown that at ambient temperature, monobromo−Mn(II) compounds are undetectable (except at very high concentrations ∼6 *m*) but as one proceeds to subcritical water at 325 °C the manganese becomes largely a tetrahedral dibromo compound. The change to [Mn(II)$(H_2O)_2$-Br_2] is essentially complete in supercritical water at 400 °C. Thus, in ambient water, the *K* in rxn 10 is close to 0, whereas at 325 °C it is high, and even higher at 400 °C. The large degree of contact ion pairs at these temperatures is not unexpected because the dielectric constant at 300 °C is 21 and at 400 °C is 7.0 which are similar to those in acetic acid, see Table 4. Hence, it is not surprising that the reported yields and selectivities in the synthesis of terephthalic acid from *p*-xylene[3] in water are significant, starting at 300 °C, and have their maximum reported values at 400 °C. The third example is consistent with our observation that at very high concentrations (e.g., 6 *m*), Mn−Br contact ion pairs are seen in ambient water.[13] Similarly, at high concentrations the oxidative synthesis of terephthalic acid from *p*-xylene proceeds even in subcritical water at 180−220 °C but requires a very high Co/Mn/Br catalyst concentration of approximately 0.3 *m*.

Conclusions

Because of its commercial importance, the chemistry and mechanisms of metal/bromide-catalyzed autoxidation in acetic acid/water solutions has been intensely studied for the last 44 years. There are at least 30 different catalysts reported in 22 different carboxylic acid solvents, and these have been applied to at least 251 different substrates. A careful detailed study of the catalytic and process chemistry has led to numerous improvements of the commercial processes as evidenced by the massive academic and patent literature.[27] Oxidation of organic substrates in scH_2O to carbon dioxide has been practiced for many years, but *selective* oxidation was reported only in the year 1998. The importance of selective oxidation in scH_2O cannot be overemphasized because the elimination of acetic acid results in large byproduct reduction and much greater energy and engineering simplification.[1,2,4] The EXAFS and XANES results in this contribution provide the first glimpse into the chemistry of the oxidation science in scH_2O by reporting several new findings related to (1) the structure of the $MnBr_2$ catalyst in scH_2O, (2) the surprising result that precipitation of the catalyst occurs by addition of the acetate anion, and (3) by the first suggestions of the types of solvent properties which are necessary for catalytic activity.

Apparently an important criterion for autoxidation activity using metal/bromide catalysts is the formation of contact ion pairs between Mn(II) and the bromide. Thus, in ambient water with its high dielectric constant of 80, no Mn−Br bonds exist, and poor catalytic activity results. At 400 °C in scH_2O at a dielectric constant of near 7, all of the bromide present (up to a ratio of at least 2/1 Br/Mn) is bound to the Mn(II), and high selective activity occurs. This result is analogous to acetic acid/water mixtures in which the catalytic activity is inversely proportional to the dielectric constant and thus proportional to

(49) Gray, H. B.; Langford, C. H. *Chem. & Engin. News* **1968**, *46*, 68.

Table 4. Relationship between Catalytic Activity and Metal−Bromide Species in Acetic Acid/Water Mixtures

water concn (wt %)	dielectric constant[50]	metal as metal–bromide species (%)	rate of oxidation of *p*-toluic acid using Co/Mn/Br catalyst (cm^3O_2/ min)[51]	rate of oxidation of 4-Cl toluene using Co/Mn/Br catalyst (cm^3O_2/ min)[51]
0	6.21	89[52]	4.8	5.5
1	7.62	67[51]	–	–
5	13.32	14[51]	2.1	3.7
10	17	3[51]	1.2	1.4

the amount of contact ion pairing of Mn(II) and Br^{-1}. A simple model is presented to rationalize these results.

This contribution also demonstrates that the chemistry involving the catalyst species in scH_2O will be subtly different than in acetic acid-based metal/bromide autoxidation. Thus, while formation of Mn(II) oxide in acetic acid-based systems is unknown, it does occur in scH_2O. And while Mn(II) acetate salts are very stable and soluble in acetic acid or in non-scH_2O, they are not in scH_2O because they form insoluble Mn(II) oxide. This chemistry also suggests that the $MnBr_2$ catalyst *may not* be the most effective catalyst as is currently suggested. This may not be true because only metal bromides, i.e., $M(N)Br_n$ (where N is the oxidation state of the metal), have been evaluated. This invariably has led to high bromide/metal ratios which may not be optimum as has been found in acetic acid-based autoxidation.[27] Attempts to change this ratio by the use of acetate has led to Mn(II) oxide formation as just described. This suggests new studies using other anions of the metal salts might be fruitful. It is likely then that manganese might not be the optimum metal and that perhaps combinations of metals, which are abundant in acetic acid−base systems,[27] may be more effective.

The high catalytic activity in scH_2O with its unusual physical properties may not lie solely with the metal-catalyzed pathways but may also promote the nonmetal-catalyzed pathways as given in rxns 2−4 above. Another result of the decreased dielectric constant in scH_2O, as compared to non-scH_2O, is a decrease in hydrogen bonding[53] in the former. It is known that hydrogen bonding to the transient peroxo radicals decreases their reactivity which is one of the reasons that water deactivates acetic-acid based autoxidation.[54] Therefore deactivation of the transient peroxy radicals may be less or absent in scH_2O than in non-scH_2O.

Finally, catalyst chemistry in the current acetic acid-based process is easily studied since the reactions can be performed in low-pressure reactors. For example, abrupt changes in overall oxidation rate can often be correlated to visual or spectroscopic changes that are easily available to the experimenter. This is generally impossible with autoxidation in scH_2O because an apparatus must be constructed to withstand very high temperatures and pressures. This study then highlights the power of in situ XAFS to derive a wide range of information on the state of the catalyst.

Acknowledgment. This work was supported by the Office of Science, Office of Basic Energy Sciences, Chemical Sciences Division of the U.S. Department of Energy (DOE). The Pacific Northwest National Laboratory is operated by Battelle for DOE. PNC-CAT facilities and research at these facilities are supported by the U.S. DOE Office of Science Grant No. DEFG03-97ER45628. Use of the Advanced Photon Source was supported by the U.S. Department of Energy, Office of Science, Office of Basic Energy Sciences, under Contract No. W-31-109-ENG-38.

Supporting Information Available: XAFS spectra of Mn oxides. This material is available free of charge via the Internet at http://pubs.acs.org.

JA053421V

(50) Popov, A. I. In *The Chemistry of Nonaqueous Solvents III*; Lagowski, J. J., Ed.; Academic Press: New York, 1970; p 214.
(51) Partenheimer, W. *J. Mol. Catal. A-Chemical* **2001**, *174*, 29.
(52) Sawada, K.; Tanaka, M. *J. Inorg. Nucl. Chem.* **1973**, *35*, 2455.
(53) Akiya, N.; Savage, P. E. *Chem. Rev.* **2002**, *102*, 2725.
(54) Ukegawa, K.; Kamiya, Y. *Bull. Chem. Soc. Jpn.* **1976**, *49*, 1632.